HHS Public Access

Author manuscript

J Am Chem Soc. Author manuscript; available in PMC 2023 February 02.

Published in final edited form as:

J Am Chem Soc. 2022 February 02; 144(4): 1534–1538. doi:10.1021/jacs.1c12506.

Organometallic $Fe_2(\mu\text{-}SH)_2(CO)_4(CN)_2$ Cluster Allows the Biosynthesis of the [FeFe]-Hydrogenase with Only the HydF Maturase

Yu Zhang[§],
School of Chemical Sciences, University of Illinois at Urbana—Champaign, Urbana, Illinois 61801, United States

Lizhi Tao[§],
Department of Chemistry, University of California, Davis, California 95616, United States

Toby J. Woods,
School of Chemical Sciences, University of Illinois at Urbana—Champaign, Urbana, Illinois 61801, United States

R. David Britt,
Department of Chemistry, University of California, Davis, California 95616, United States

Thomas B. Rauchfuss
School of Chemical Sciences, University of Illinois at Urbana—Champaign, Urbana, Illinois 61801, United States

Abstract

The biosynthesis of the active site of the [FeFe]-hydrogenases (HydA1), the H-cluster, is of interest because these enzymes are highly efficient catalysts for the oxidation and production of H_2. The biosynthesis of the $[2Fe]_H$ subcluster of the H-cluster proceeds from simple precursors, which are processed by three maturases: HydG, HydE, and HydF. Previous studies established that HydG produces an $Fe(CO)_2(CN)$ adduct of cysteine, which is the substrate for HydE. In this work, we show that by using the synthetic cluster $[Fe_2(\mu\text{-}SH)_2(CN)_2(CO)_4]^{2-}$ active HydA1 can be biosynthesized without maturases HydG and HydE.

Corresponding Authors R. David Britt – Department of Chemistry, University of California, Davis, California 95616, United States; rdbritt@ucdavis.edu; **Thomas B. Rauchfuss** – School of Chemical Sciences, University of Illinois at Urbana—Champaign, Urbana, Illinois 61801, United States; rauchfuz@illinois.edu.

[§]Author Contributions
Y.Z. and L.T. contributed equally to this work.

Supporting Information
The Supporting Information is available free of charge at https://pubs.acs.org/doi/10.1021/jacs.1c12506.
Synthetic procedures, NMR spectrum, additional IR spectrum, X-ray crystallography, *in vitro* maturation, EPR spectroscopy, H_2 production assay, and DFT calculations (PDF)

Accession Codes
CCDC 2111350 and 2111351 contain the supplementary crystallographic data for this paper. These data can be obtained free of charge via www.ccdc.cam.ac.uk/data_request/cif, or by emailing data_request@ccdc.cam.ac.uk, or by contacting The Cambridge Crystallographic Data Centre, 12 Union Road, Cambridge CB2 1EZ, UK; fax: + 44 1223 336033.

The authors declare no competing financial interest.

As highly efficient catalysts for the redox chemistry of H_2, both its oxidation and its production from protons, the [FeFe]-hydrogenases have attracted much attention.[1-3] Knowledge of these enzymes inspires the design of catalysts relevant to fuel cells and thus sustainable energy.[4] The fact that the catalytic active site of these enzymes is iron-based makes this quest especially enticing.[5] While our understanding of how [FeFe]-hydrogenases function is substantial, major gaps remain as to how nature makes the remarkable active site.[6,7] Understanding these steps promises to reveal new organometallic chemistry and could even underpin rational methods for modifying these enzymes.

The catalytic H-cluster consists of a canonical $[4Fe—4S]_H$ subcluster linked through a bridging cysteine (Cys) residue to a diiron subcluster.[1] This subcluster, called $[2Fe]_H$, is the active site for the substrate H^+/H_2 binding and activation.[8] Although simple in stoichiometry, $[2Fe]_H$ features unusual cofactors (CO, CN^-, and $(SCH_2)_2NH^{2-}$ (azadithiolate, adt)) and an Fe—Fe bond. Three maturation enzymes, HydG, HydE, and HydF, are responsible for the synthesis of $[2Fe]_H$ (Figure 1).[6,7] Although consensus is lacking for the full biosynthetic pathway, it is widely agreed that the process starts with HydG. This radical *S*-adenosyl-L-methionine (rSAM) enzyme produces CN^- and CO via the cleavage of tyrosine.[9-11] Of overarching interest is the assembly of the Fe_2S_2 core of the $[2Fe]_H$ subcluster. One hypothesis proposes that $[2Fe]_H$ is derived by retrofitting a typical preformed cysteine-ligated [2Fe—2S] cluster with free CO and CN^-.[12] We have proposed that $[2Fe]_H$ is derived from $[Fe^{II}(CN)(CO)_2(cysteine)]^-$.[13] Termed complex B, this cysteine–Fe complex is the product of HydG[11,13,14] and the substrate of HydE.[15,16] The HydE maturase, also an rSAM enzyme, reduces the low-spin Fe(II) center of complex B to Fe(I) via a radical mechanism, followed by dealkylation to form a mononuclear $Fe^IS(CN)(CO)_2$ entity.[15,16] It has recently been speculated that a pair of these Fe(I) entities dimerize to generate an immature Fe_2S_2 cluster (Figure 1A), which is released by HydE and further processed by HydF for the installation of the bridging $NH(CH_2)_2$. A stringent test of this combination/dimerization hypothesis would entail the demonstration that a synthetic Fe_2S_2 cluster species allows the biosynthesis of active hydrogenase in the absence of HydG and HydE. In this communication, we provide such evidence.

The key Fe_2S_2 species was prepared from $K[Fe(CN)(CO)_4]$ (K[**1**], Figure S7). Related salts of $[Fe(CN)(CO)_4]^-$ have long been known,[17,18] but this inorganic salt has distinctive solubility characteristics, being soluble in diethyl ether and producing derivatives that are water-soluble as required for biosynthetic experiments. Typical of other iron carbonyls, the CO ligands in $[Fe(CN)(CO)_4]^-$ are labilized upon ultraviolet (UV) light irradiation.[19] This allows for the introduction of the inorganic sulfur ligands, providing access to Fe—S—CN—CO assemblies. Such species have been invoked as intermediates in the iron–sulfur hypothesis of the origin of life.[20]

Irradiating an ether—pentane solution of $K[Fe(CN)(CO)_4]$ with monochromatic 365 nm light under an atmosphere of H_2S resulted in a complicated mixture. A series of crystallizations and extractions culminating with the addition of the crown ether (18-crown-6) gave the salt $[K_2(18\text{-crown-6})_2(thf)][Fe_2(\mu\text{-}SH)_2(CN)_2(CO)_4]$ ($[K_2(18\text{-c-6})_2(thf)][\mathbf{2}]$) in 8% yield. We propose that $[\mathbf{2}]^{2-}$ arises from the dehydrogenative dimerization of $[Fe^{II}(SH)(H)]$ species, analogous to Darensbourg's synthesis of $Fe_2(\mu\text{-}SPh)_2(CO)_6$ by the

protonation of $[Fe(SPh)(CO)_4]^-$. [21] The low yield (8%) of our synthesis contrasts with the efficiency of the biosynthesis, which also proceeds by the dimerization of two Fe—S—$(CO)_2$—CN species within HydE.[16]

The Fourier transform infrared (FTIR) spectrum of solid $[K_2(18\text{-c-}6)_2(thf)][\mathbf{2}]$ shows a weak band at 2501 cm^{-1}, which is assigned to ν_{SH} (Figure S11).[22] The bands for ν_{CN} (m, 2080 cm^{-1}) and ν_{CO} (s, 1971, 1931, 1893 cm^{-1}) in acetonitrile (Figure 2B) are similar to those for $[Fe_2(adt)\text{-}(CN)_2(CO)_4]^{2-}$.[23] Fe—SH clusters, although rare, have been discussed as intermediates for dinitrogen fixation by the nitrogenases.[24]

The structure of $[K_2(18\text{-c-}6)_2(thf)][\mathbf{2}]$ was established by X-ray crystallography (Figure 2A). In the solid-state structure, the two cyanide ligands are readily distinguished from CO by their Fe—CN distances, which are 0.194 Å longer than the Fe—CO bonds. Furthermore, both cyanide ligands bond to $K(18\text{-crown-}6)^+$ centers, reminiscent of the tendency of FeCN groups in HydA1 to engage in hydrogen bonds.[25] The cyanide ligands occupy apical positions. This stereochemistry is typical for other derivatives of the type $[Fe^I_2(SR)_2(CO)_{6-x}L_x]$ but differs from the situation for the $[2Fe]_H$ cluster where the two cyanides are equatorial. The metal–ligand and metal–metal distances are statistically indistinguishable from those for $[Fe_2(adt)(CN)_2(CO)_4]^{2-}$. The S—H centers, which were located and refined isotropically, are both axial (aa isomer). In solution, however, the axial–equatorial (ae) isomer predominates, as is normally observed[26] and as predicted computationally (Figure S15). A third isomer of $[\mathbf{2}]^{2-}$ is detected by ^1H NMR spectroscopy ($\delta_{SH\text{-}ee} = -1.78$) as well, consistent with a diequatorial (ee) isomer (Figure 3). In the ae isomer, the CO ligands are diastereotopic, which was confirmed by ^{13}C NMR analysis showing two ^{13}CO ($\delta_{CO\text{-}ae}$ = 222, 221) signals and one ^{13}CN ($\delta_{CN\text{-}ae}$ = 149) signal.

The biochemical phase of this work commenced with testing the possibility that synthetic $[\mathbf{2}]^{2-}$ can replace HydG and HydE maturases in the biosynthesis of the H-cluster, i.e., *in vitro* HydG/HydE-less maturation. Only the HydF maturase, apo-*Cr*HydA1 (that harbors a $[4Fe—4S]_H$ subcluster), $[K_2(18\text{-c-}6)_2(thf)][\mathbf{2}]$, *E. coli* cell lysate, pyridoxal phosphate (PLP), and guanosine triphosphate (GTP) (details in the Supporting Information) were included in the maturation. Indeed, this HydG/HydE-less medium allows the biosynthesis of *Cr*HydA1 with H_2 production activity comparable to that of the standard holo-*Cr*HydA1 (Figure 1B). Our *in-vitro*-assembled H-cluster was interrogated by electron paramagnetic resonance (EPR) spectroscopy. Both the H_{ox} and H_{ox}—CO (the CO-inhibited form) states are mixed-valence $S = 1/2$ systems, which are ideally suited for EPR investigation. As shown in Figure 4A, the EPR spectrum of the resulting $[\mathbf{2}]^{2-}$-*Cr*HydA1 poised in the thionine-oxidized state exhibits a rhombic signal with a **g** tensor of $[g_1, g_2, g_3]$ = [2.103, 2.041, 1.998], characteristic of H_{ox}. H_{ox}-CO is also observed with its typical axial signal with a **g** tensor of [2.055, 2.009, 2.007], as routinely observed in *in-vitro*-maturated hydrogenase samples[13,27,28] as well as $[Fe_2(adt)(CN)_2(CO)_4]^{2-}$-maturated hydrogenases.[29] This finding strongly implies that the H-cluster is assembled from an $Fe_2(SH)_2$ precursor.

To further support the above results, the maturation was conducted with $[\mathbf{2}]^{2-}$ wherein both cyanide ligands are ^{13}CN-labeled (^{13}CN-$[\mathbf{2}]^{2-}$). The isotopologues ^{12}CN-$[\mathbf{2}]^{2-}$ and ^{13}CN-$[\mathbf{2}]^{2-}$ are readily distinguished by their FTIR spectra as the ν_{CN} band shifted to lower

energy by 45 cm^{-1} as compared to naturally abundant [**2**]$^{2-}$, while the ν_{CO} bands are almost unchanged (Figure 2B). The ^{13}C NMR spectrum of ^{13}CN-[**2**]$^{2-}$ shows three signals in the ^{13}CN region with integrated intensities matching those of isomers assigned by the SH signals in the ^{1}H NMR spectrum (Figures S5 and S6). HydG/HydE-less maturation using ^{13}CN-[**2**]$^{2-}$ generated the corresponding ^{13}CN-[**2**]$^{2-}$-*Cr*HydA1 as the exclusive EPR-detectable product once oxidized by thionine. The EPR spectrum (Figure 4E) of the ^{13}CN-labeled H_{ox} sample clearly shows ~30 MHz hyperfine splitting, which is identical to the hyperfine splitting observed from the ^{13}CN-labeled H-cluster.[13] The constitution of HydA1 derived from ^{13}C-[**2**]$^{2-}$ was further characterized by electron–nuclear double-resonance (ENDOR) spectroscopy. Measurements were recorded at Q-band EPR frequencies (~34 GHz) using the Davies ENDOR sequence to characterize the hyperfine coupling between the ^{13}C magnetic nuclei and the electron spin center (i.e., the distal Fe center in the H_{ox} state). Two inequivalent hyperfine-coupled ^{13}C nuclei are detected (Figure 4F) and are assigned to the distal and proximal ^{13}CN sites (Figure 4G), with hyperfine tensors of [30.2, 26.2, 29.0] and [5.26, 5.24, 4.46] MHz, respectively, that match our previous studies of the ^{13}CN-labeled H_{ox} state (Figure S12).[30] This result clearly indicates that the CN^- ligands in the H-cluster come from [**2**]$^{2-}$, which is consistent with the role of [**2**]$^{2-}$ as a competent organometallic precursor to the H-cluster.

Implicit in our HydG/HydE-less maturation of HydA1 is that the bridging $HN(CH_2)_2$ group is installed on the $Fe_2(SH)_2$ core. This scenario was confirmed by the maturation of [**2**]$^{2-}$ using 3-^{13}C/^{15}N-labeled serine in the medium,[6,7] as our previous work[28] had identified 3-C and N of serine as the source of the respective C and N centers of the bridging $HN(CH_2)_2$ group.[6,7] As observed by ^{13}C/^{15}N Mims-ENDOR (Figure 4B,C), two sets of ^{13}C hyperfine coupling interactions (A(^{13}C1) = [3.40, 1.35, 1.37] MHz and *A*(^{13}C2) = [0.28, 1.32, 1.28] MHz) and one ^{l5}N hyperfine coupling interaction (*A*(^{15}N) = [1.90, 1.57, 1.63] MHz), as illustrated in Figure 4D are detected by recording the ENDOR spectra at magnetic field positions corresponding to the g_1 and g_3 of H_{ox}, where there are no contributions from the H_{ox}-CO EPR signal. These hyperfine couplings are identical to previously reported values (Figure S12).[28,31,32] All results show that [**2**]$^{2-}$ is a competent precursor en route to the H-cluster.

An additional control experiment, omitting HydF from HydG/HydE-less maturation, resulted in no assembled H-cluster in the HydA1 sample (Figure S13), which consequently exhibited no H_2 production activity (Figure 1B). Clearly, HydF plays an essential role in transforming [**2**]$^{2-}$ into the H-cluster.

In summary, insights into the biosynthesis of the H-cluster are provided by a synthetic Fe_2S_2 cluster, which allows the *in vitro* production of active [FeFe]-hydrogenase in the presence of only one maturase, HydF. These results help to define a roadmap for the biosynthesis of the [FeFe]-hydrogenase by three maturases : HydG produces [Fe^{II}(CN)-$(CO)_2$(cysteine)]$^-$, HydE converts this synthon into $[Fe_2(SH)_2(CN)_2(CO)_4]^{2-}$, and HydF installs the amine cofactor.

Supplementary Material

Refer to Web version on PubMed Central for supplementary material.

ACKNOWLEDGMENTS

This work was supported by NIH grants GM61153 (to T.B.R.) and 1R35GM126961-01 (to R.D.B.). We thank Dr. Kundan Singh for preliminary synthetic experiments.

REFERENCES

(1). Lubitz W; Ogata H; Rüdiger O; Reijerse E Hydrogenases. Chem. Rev 2014, 114, 4081–4148. [PubMed: 24655035]

(2). Kleinhaus JT; Wittkamp F; Yadav S; Siegmund D; Apfel U-P [FeFe]-Hydrogenases: Maturation and Reactivity of Enzymatic Systems and Overview of Biomimetic Models. Chem. Soc. Rev 2021, 50, 1668–1784. [PubMed: 33305760]

(3). Land H; Senger M; Berggren G; Stripp ST Current State of [FeFe]-Hydrogenase Research: Biodiversity and Spectroscopic Investigations. ACS Catal. 2020, 10, 7069–7086.

(4). Evans RM; Siritanaratkul B; Megarity CF; Pandey K; Esterle TF; Badiani S; Armstrong FA The Value of Enzymes in Solar Fuels Research – Efficient Electrocatalysts Through Evolution. Chem. Soc. Rev 2019, 48, 2039–2052. [PubMed: 30426997]

(5). Bullock RM; Chen JG; Gagliardi L; Chirik PJ; Farha OK; Hendon CH; Jones CW; Keith JA; Klosin J; Minteer SD; Morris RH; Radosevich AT; Rauchfuss TB; Strotman NA; Vojvodic A; Ward TR; Yang JY; Surendranath Y Using Nature's Blueprint to Expand Catalysis with Earth-Abundant Metals. Science 2020, 369, eabc3183. [PubMed: 32792370]

(6). Britt RD; Rao G; Tao L Biosynthesis of the Catalytic H-Cluster of [FeFe] Hydrogenase: the Roles of the Fe—S Maturase Proteins HydE, HydF, and HydG. Chem. Sci 2020, 11, 10313–10323. [PubMed: 34123177]

(7). Britt RD; Rao G; Tao L Bioassembly of Complex Iron–Sulfur Enzymes: Hydrogenases and Nitrogenases. Nat. Rev. Chem 2020, 4, 542–549. [PubMed: 33829110]

(8). Reijerse EJ; Pham CC; Pelmenschikov V; Gilbert-Wilson R; Adamska-Venkatesh A; Siebel JF; Gee LB; Yoda Y; Tamasaku K; Lubitz W; Rauchfuss TB; Cramer SP Direct Observation of an Iron-Bound Terminal Hydride in [FeFe]-Hydrogenase by Nuclear Resonance Vibrational Spectroscopy. J. Am. Chem. Soc 2017, 139, 4306–4309. [PubMed: 28291336]

(9). Shepard EM; Duffus BR; George SJ; McGlynn SE; Challand MR; Swanson KD; Roach PL; Cramer SP; Peters JW; Broderick JB [FeFe]-Hydrogenase Maturation: HydG-Catalyzed Synthesis of Carbon Monoxide. J. Am. Chem. Soc 2010, 132, 9247–9249. [PubMed: 20565074]

(10). Driesener RC; Challand MR; McGlynn SE; Shepard EM; Boyd ES; Broderick JB; Peters JW; Roach PL [FeFe]-Hydrogenase Cyanide Ligands Derived from *S*-Adenosylmethionine-Dependent Cleavage of Tyrosine. Angew. Chem., Int. Ed 2010, 49, 1687–1690.

(11). Kuchenreuther JM; Myers WK; Suess DLM; Stich TA; Pelmenschikov V; Shiigi SA; Cramer SP; Swartz JR; Britt RD; George SJ The HydG Enzyme Generates an $Fe(CO)_2(CN)$ Synthon in Assembly of the FeFe Hydrogenase H-Cluster. Science 2014, 343, 424–427. [PubMed: 24458644]

(12). Shepard EM; McGlynn SE; Bueling AL; Grady-Smith CS; George SJ; Winslow MA; Cramer SP; Peters JW; Broderick JB Synthesis of the 2Fe Subcluster of the [FeFe]-Hydrogenase H Cluster on the HydF Scaffold. Proc. Natl. Acad. Sci. U.S.A 2010, 107, 10448–10453. [PubMed: 20498089]

(13). Rao G; Pattenaude SA; Alwan K; Blackburn NJ; Britt RD; Rauchfuss TB The Binuclear Cluster of [FeFe] Hydrogenase is Formed with Sulfur Donated by Cysteine of an $[Fe(Cys)\text{-}(CO)_2(CN)]$ Organometallic Precursor. Proc. Natl. Acad. Sci. U.S.A 2019, 116, 20850–20855. [PubMed: 31570604]

(14). Suess DLM; Bürstel I; De La Paz L; Kuchenreuther JM; Pham CC; Cramer SP; Swartz JR; Britt RD Cysteine as a Ligand Platform in the Biosynthesis of the FeFe Hydrogenase H Cluster. Proc. Natl. Acad. Sci. U.S.A 2015, 112, 11455–11460. [PubMed: 26324916]

(15). Tao L; Pattenaude SA; Joshi S; Begley TP; Rauchfuss TB; Britt RD Radical SAM Enzyme HydE Generates Adenosylated Fe(I) Intermediates en Route to the [FeFe]-Hydrogenase Catalytic H-Cluster. J. Am. Chem. Soc 2020, 142, 10841–10848. [PubMed: 32434327]

(16). Rohac R; Martin L; Liu L; Basu D; Tao L; Britt RD; Rauchfuss TB; Nicolet Y Crystal Structure of the [FeFe]-Hydrogenase Maturase HydE Bound to Complex-B. J. Am. Chem. Soc 2021, 143, 8499–8508. [PubMed: 34048236]

(17). Ruff JK Chemistry of Dinuclear Carbonyl Anions. IV. Thiocyanate- and Cyanide-Bridged Complexes. Inorg. Chem 1969, 8, 86–89.

(18). Goldfield SA; Raymond KN Axial *vs.* Equatorial Bonding in Trigonal-Bipyramidal Complexes. Crystal and Molecular Structure of [Bis(triphenylphosphine) imminium]tetracarbonylcyanideiron(0), $[((C_6H_5)_3P)_2N][Fe(CO)_4CN]$. Inorg. Chem 1974, 13, 770–775.

(19). Kayal A; Rauchfuss TB Protonation Studies of the New Iron Carbonyl Cyanide *trans*-$[Fe(CO)_3(CN)_2]^{2-}$: Implications with Respect to Hydrogenases. Inorg. Chem 2003, 42, 5046–5048. [PubMed: 12924874]

(20). Wächtershäuser G From Chemical Invariance to Genetic Variability in Bioinspired Catalysis; Weigand W, Schollhammer P, Eds.; Wiley-VCH: Weinheim, 2014; pp 1–20.

(21). Liaw W-F; Kim C; Darensbourg MY; Rheingold AL Thiolate, Thioether, and Thiol Derivatives of Iron(0) Carbonyls. J. Am. Chem. Soc 1989, 111, 3591–3597.

(22). Pluth MD; Tonzetich ZJ Hydrosulfide Complexes of the Transition Elements: Diverse Roles in Bioinorganic, Cluster, Coordination, and Organometallic Chemistry. Chem. Soc. Rev 2020, 49, 4070–4134. [PubMed: 32420562]

(23). Berggren G; Adamska A; Lambertz C; Simmons TR; Esselborn J; Atta M; Gambarelli S; Mouesca JM; Reijerse E; Lubitz W; Happe T; Artero V; Fontecave M Biomimetic Assembly and Activation of [FeFe]-Hydrogenases. Nature 2013, 499, 66–69. [PubMed: 23803769]

(24). Hoffman BM; Lukoyanov D; Yang Z-Y; Dean DR; Seefeldt LC Mechanism of Nitrogen Fixation by Nitrogenase: the Next Stage. Chem. Rev 2014, 114, 4041–4062. [PubMed: 24467365]

(25). Nicolet Y; Lemon BJ; Fontecilla-Camps JC; Peters JW A Novel FeS Cluster in Fe-only Hydrogenases. Trends Biochem. Sci 2000, 25, 138–143. [PubMed: 10694885]

(26). Kagalwala HN; Lalaoui N; Li Q-L; Liu L; Woods T; Rauchfuss TB Redox and "Antioxidant" Properties of $Fe_2(\mu\text{-}SH)_2(CO)_4(PPh_3)_2$. Inorg. Chem 2019, 58, 2761–2769. [PubMed: 30724559]

(27). Rao G; Britt RD Electronic structure of two Catalytic States of the [FeFe] Hydrogenase H-Cluster as Probed by Pulse Electron Paramagnetic Resonance Spectroscopy. Inorg. Chem 2018, 57, 10935–10944. [PubMed: 30106575]

(28). Rao G; Tao L; Britt RD Serine is the Molecular Source of the $NH(CH_2)_2$ Bridgehead Moiety of the *in vitro* Assembled [FeFe] Hydrogenase H-Cluster. Chem. Sci 2020, 11, 1241–1247.

(29). Németh B; Esmieu C; Redman HJ; Berggren G Monitoring H-Cluster Assembly Using a Semi-Synthetic HydF Protein. Dalton Trans. 2019, 48, 5978–5986. [PubMed: 30632592]

(30). Myers WK; Stich TA; Suess DLM; Kuchenreuther JM; Swartz JR; Britt RD The Cyanide Ligands of [FeFe] Hydrogenase: Pulse EPR Studies of ^{13}C and ^{15}N-Labeled H-Cluster. J. Am. Chem. Soc 2014, 136, 12237–12240. [PubMed: 25133957]

(31). Reijerse EJ; Pelmenschikov V; Birrell JA; Richers CP; Kaupp M; Rauchfuss TB; Cramer SP; Lubitz W Asymmetry in the Ligand Coordination Sphere of the [FeFe] Hydrogenase Active Site is Reflected in the Magnetic Spin Interactions of the Aza-propanedithiolate Ligand. J. Phys. Chem. Lett 2019, 10, 6794–6799. [PubMed: 31580680]

(32). Adamska-Venkatesh A; Roy S; Siebel JF; Simmons TR; Fontecave M; Artero V; Reijerse E; Lubitz W Spectroscopic Characterization of the Bridging Amine in the Active Site of [FeFe] Hydrogenase Using Isotopologues of the H-Cluster. J. Am. Chem. Soc 2015, 137, 12744–12747. [PubMed: 26393426]

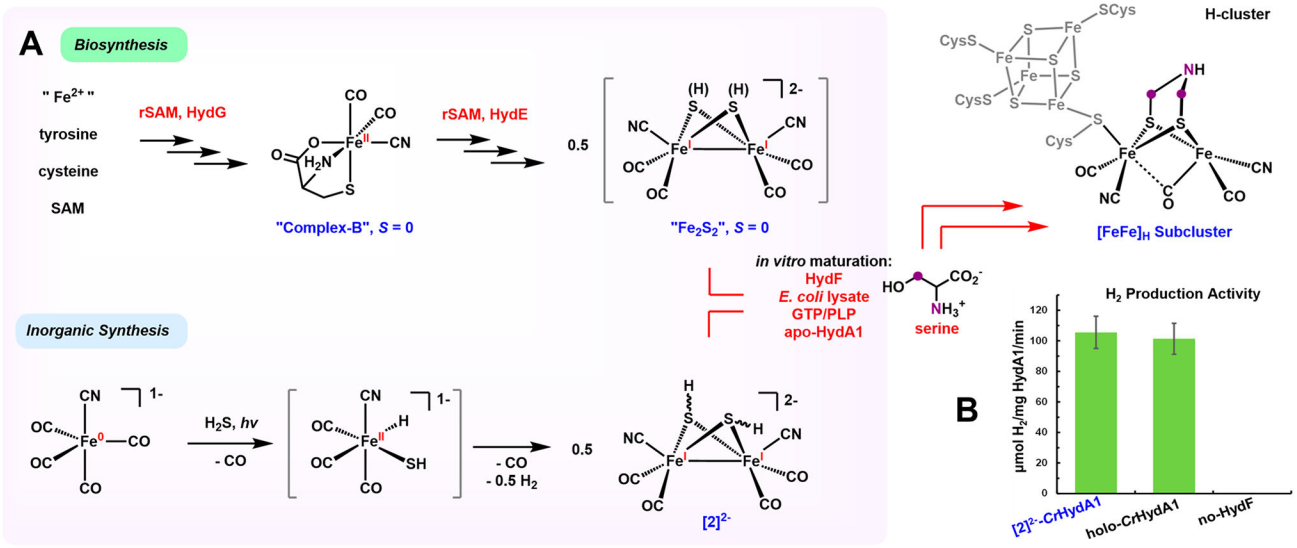

Figure 1.

(A) Proposed biological and inorganic synthetic pathways for the assembly of the [FeFe]-hydrogenase H-cluster. (B) H_2 production activity (20 °C) of [**2**]$^{2-}$-*Cr*HydA1, holo-*Cr*HydA1, and an inactive maturated sample omitting the HydF maturase from the *in vitro* HydG/HydE-less maturation.

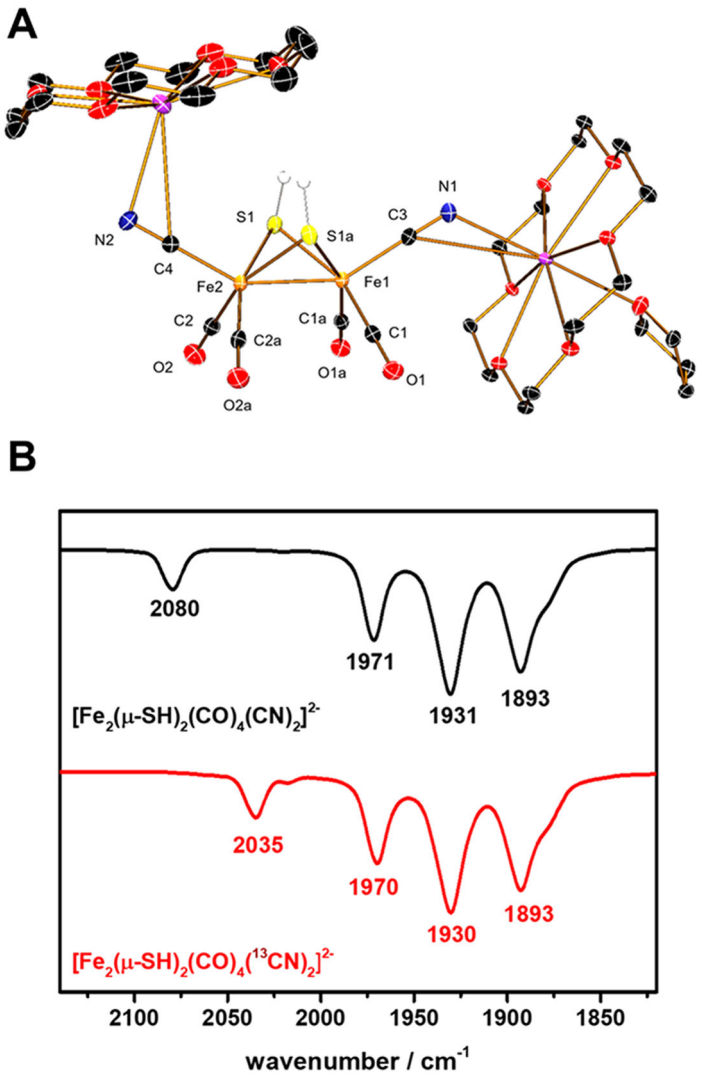

Figure 2.

(A) Structure of $[K_2(18\text{-c-}6)_2(thf)]$[**2**]. Non-SH protons were omitted for clarity. (B) FTIR spectrum of $[K_2(18\text{-c-}6)_2(thf)]$[**2**] (black) and $[K_2(18\text{-c-}6)_2(thf)]$-^{13}CN-[**2**] (red) in acetonitrile under N_2.

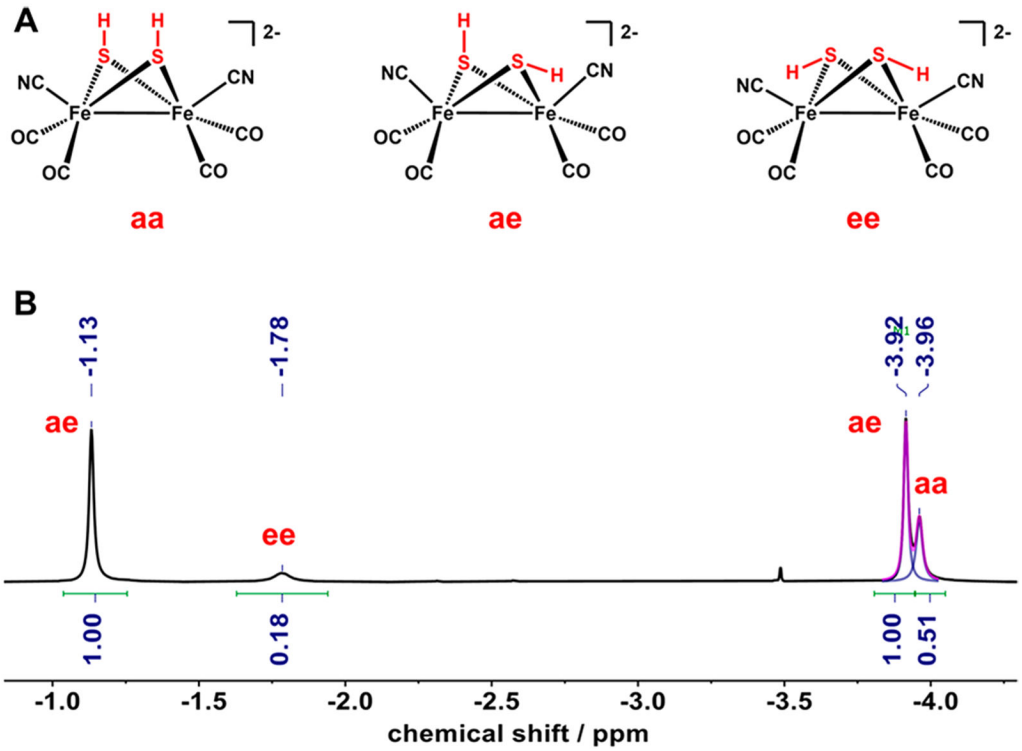

Figure 3.

(A) Isomers for $[\mathbf{2}]^{2-}$. (B) ^{1}H NMR spectrum (high-field region) of $[K_2(18\text{-c-}6)_2(thf)][\mathbf{2}]$ in CD_3CN solution.

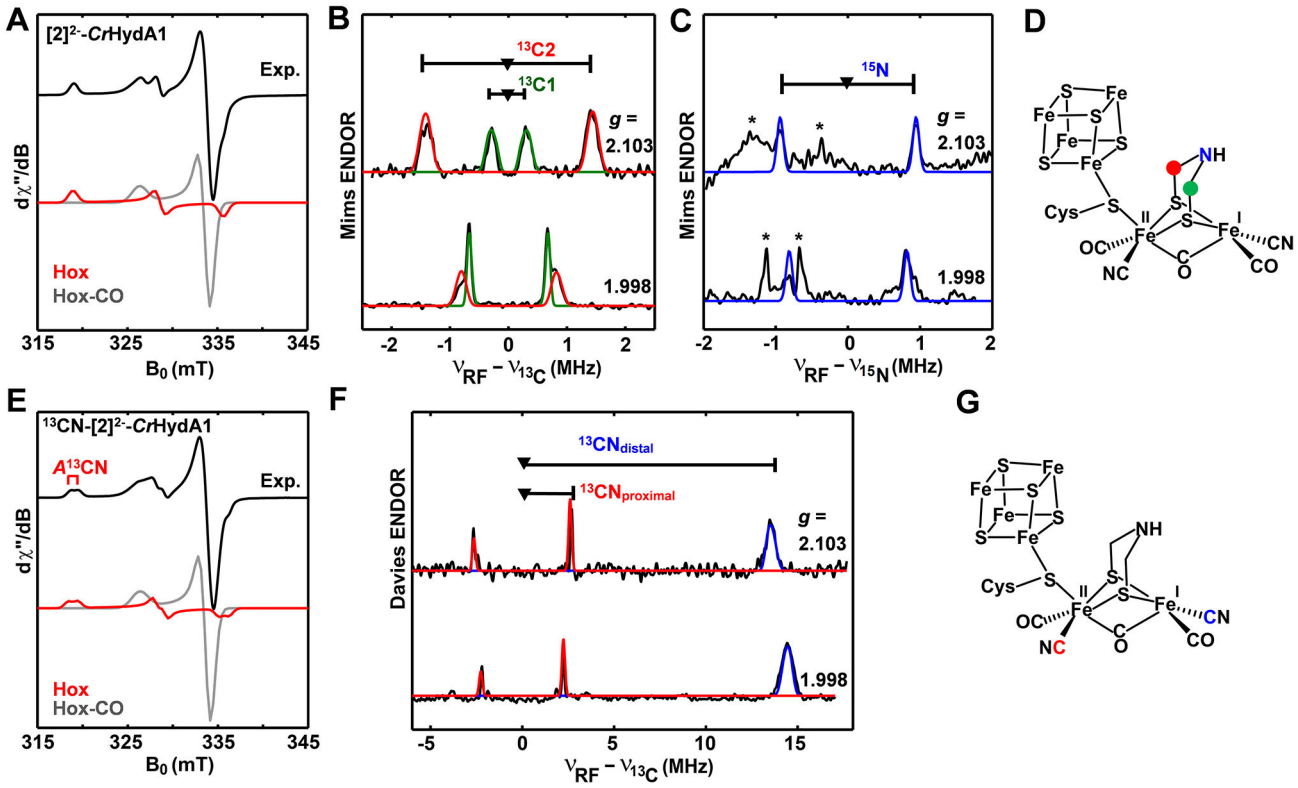

Figure 4.

EPR spectroscopic characterization of *Cr*HydA1 maturated with [**2**]$^{2-}$. X-band continuous-wave (CW) EPR spectra (15 K) of (A) [**2**]$^{2-}$-*Cr*HydA1 and (E) ^{13}CN-[**2**]$^{2-}$-*Cr*HydA1 oxidized by thionine. Both spectra are simulated using two components: H_{ox} in red with **g** = [2.103, 2.041, 1.998] and Hox-CO in gray with **g** = [2.055, 2.009, 2.007]. (B) Q-band ^{13}C- and (C) ^{15}N-Mims ENDOR spectra of [**2**]$^{2-}$-*Cr*HydA1 with the isotopically labeled $^{15}NH(^{13}CH_2)_2$ bridgehead as illustrated in (D). (F) Q-band ^{13}C-Davies ENDOR spectra of ^{13}CN-[**2**]$^{2-}$-*Cr*HydA1, as illustrated in (G). The ENDOR spectra were recorded at 15 K and at the magnetic field positions corresponding to g_1 = 2.103 and g_3 = 1.998 of H_{ox}, where there are no EPR signal contributions from H_{ox}-CO. The black traces are experimental spectra, and the colored traces are simulated spectra (details in the Supporting Information). The ENDOR features marked by asterisks in (C) correspond to the third-order harmonics of ^{13}C ENDOR signals shown in (B).